Metal-Phosphide-Containing Porous Carbons Derived from an Ionic-Polymer Framework and Applied as Highly Efficient Electrochemical Catalysts for Water Splitting

Sheng Han, Yunlong Feng, Fan Zhang, Chongqing Yang, Zhaoquan Yao, Wuxue Zhao, Feng Qiu, Lingyun Yang, Yefeng Yao, Xiaodong Zhuang,* and Xinliang Feng*

A novel phosphorus-containing porous polymer is efficiently prepared from tris(4-vinylphenyl)phosphane by radical polymerization, and it can be easily ionized to form an ionic porous polymer after treatment with hydrogen iodide. Upon ionic exchange, transition-metal-containing anions, such as tetrathiomolybdate (MoS_4^{2-}) and hexacyanoferrate ($Fe(CN)_6^{3-}$), are successfully loaded into the framework of the porous polymer to replace the original iodide anions, resulting in a polymer framework containing complex anions (termed HT-Met, where Met = Mo or Fe). After pyrolysis under a hydrogen atmosphere, the HT-Met materials are efficiently converted at a large scale to metal-phosphide-containing porous carbons (denoted as MetP@PC, where again Met = Mo or Fe). This approach provides a convenient pathway to the controlled preparation of metal-phosphide-loaded porous carbon composites. The MetP@PC composites exhibit superior electrocatalytic activity for the hydrogen evolution reaction (HER) under acidic conditions. In particular, MoP@PC with a low loading of 0.24 mg cm^{-2} (on a glass carbon electrode) affords an *iR*-corrected (where *i* is current and *R* is resistance) current density of up to 10 mA cm^{-2} at 51 mV versus the reversible hydrogen electrode and a very low Tafel slope of 45 mV dec^{-1}, in rotating disk measurements under saturated N_2 conditions.

1. Introduction

Molecular hydrogen (H_2) is regarded as a promising energy carrier for replacing fossil fuels in the future.[1] At present the main technology for hydrogen production still consumes fossil resources and increases carbon emissions. Direct electrochemical water splitting seems to represent one of the most clean and sustainable methods for H_2-production on a large scale.[2] The hydrogen evolution reaction (HER) and the oxygen evolution reaction (OER) are the two half-cell reactions of electrochemical water splitting. Highly effcient electrochemical catalysts are required to drive the HER at low overpotentials. Catalysts based on precious metals, such as platinum, have excellent catalytic performance for the HER, but they are not suitable for wide-spread practical applications due to their expense and scarcity.[3] To date, a large number of earth-abundant electrocatalysts have been explored; they can be organized into two categories:[4] 1) metal-free heteroatom-doped carbon materials, such as materials based on carbon nanotubes,[5] graphene,[6] and graphitic carbon nitride;[7] and 2) materials evolved from transition-metal carbides, oxides, sulfides, and phosphides, such as molybdenum-,[2,8] iron-,[9] cobalt-,[10] copper-,[11] tungsten-,[12] and nickel-based materials.[13]

Typically, transition-metal-based catalysts for the HER are much superior to the metal-free catalysts. Among the reported transition-metal-based HER catalysts, transition-metal phosphides (MetPs)—such as MoP,[2,8d,f,14] Cu_3P,[11b] FeP,[9,15] Ni_2P,[13a] WP_x,[12d] and CoP_x[10a,c,e,16]—have exhibited the most promising catalytic performance, which is close to that of commercially available Pt-based catalysts However, most of the reported MetP catalysts suffer from two main limitations:[17] 1) lack of exposed active sites due to the low specific surface areas, 2) poor electrical conductivity due to the lack of favorable charge carriers. Some efforts have been made to overcome these drawbacks—for example, the formation of an interconnected network of MoP nanoparticles[8d] and of graphene sheets loaded with FeP nanoparticles,[9b] which brought about improvements in surface area and electrical conductivity, respectively. However, very few attempts have been made to explore new precursors to replace the traditional inorganic-salt sources consisting of oxygen-rich phosphorus anions (e.g., $P_xO_n^{m-}$, $HP_xO_n^{m-}$, and $H_2P_xO_n^{m-}$) and transition-metal cations (e.g., Fe^{3+}, Co^{3+}, Ni^{2+}, and Mo^{3+}).

Prof. S. Han, Y. Feng, Dr. F. Qiu
School of Chemical and Environmental Engineering
Shanghai Institute of Technology
Haiquan Road 100, 201418 Shanghai, P. R. China
Prof. F. Zhang, C. Yang, Z. Yao, W. Zhao, Dr. F. Qiu, Dr. X. Zhuang, Prof. X. Feng
School of Chemistry and Chemical Engineering
Shanghai Jiao Tong University
Dongchuan Road 800, 200240 Shanghai, P. R. China
E-mail: fan-zhang@sjtu.edu.cn; zhuang@sjtu.edu.cn
L. Yang, Prof. Y. Yao
Physics Department & Shanghai Key Laboratory of Magnetic Resonance
East China Normal University
North Zhongshan Road 3663, 200062 Shanghai, P. R. China
Prof. X. Feng
Technische Universität Dresden
Mommsenstrasse 4, 01062 Dresden, Germany

DOI: 10.1002/adfm.201501390

Herein, we present an efficient approach for preparing porous carbons embedded with transition-metal phosphides (MetP@PCs, where the transition metal center is Met = Mo, Fe) at a large scale through the direct pyrolysis of cationic, phosphorous-based, porous polymer precursors loaded with transition-metal-containing anions under a hydrogen atmosphere. The transition-metal-containing anions and phosphorous-based polymer framework serve as the metal and phosphorous sources, respectively, for the formation of the MetP@PCs under pyrolytic and reducing conditions. The as-prepared MetP@PCs process high specific surface areas of up to 451 m^2 g^{-1}. They exhibited very promising electrochemical catalytic activities for the HER in 0.5 M H_2SO_4. MoP@PC (0.24 mg cm^{-2} on a glass carbon electrode) exhibited an overpotential of 51 mV at 10 mA cm^{-2} and a Tafel slope of 45 mV dec^{-1}, comparable to those of the commercially available Pt/C catalyst (24 mV at 10 mA cm^{-2}; 30 mV dec^{-1}).

2. Results and Discussion

The strategy for the synthesis of cationic porous polymers loaded with metal-containing anions is presented in **Scheme 1**. Firstly, tris(4-vinylphenyl)phosphane[18] (TVP) was utilized as the key monomer for preparing hyper-cross-linked tri(4-vinylphenyl) phosphane (HC-TVP) through azodiisobutyronitrile (AIBN)-promoted radical polymerization. Afterwards, the resulting HC-TVP was converted to the ionic polymer (HT-I), consisting of a cationic framework and iodide counter-anions under the treatment of aqueous HI for 24 h. HT-I can be uniformly dispersed in some common organic solvents, such as dimethylformamide (DMF, 1.0 mg mL^{-1}) and dioxane. The iodide ions of HT-I can be easily replaced by metal-containing anions, such as tetrathiomolybdate (MoS_4^{2-}) and hexacyanoferrate ($Fe(CN)_6^{3-}$), by an ion-exchange process in aqueous solution. The resulting precipitate was collected and dried under vacuum, to afford the metal-containing anion-loaded cationic porous polymers (denoted as HT-Met) as a dark solid at very large scale (≈1 kg). Among the various polymers, the [MoS_4^{2-}]- and [$Fe(CN)_6^{3-}$]-loaded cationic porous polymers will be denoted as HT-Mo and HT-Fe, respectively.

In order to understand the chemical structures of the as-prepared porous polymers, HC-TVP and HT-I were characterized by solid-state NMR (SS-NMR, **Figure 1**). In ^{13}C NMR spectra (Figure 1a), the peak at 146.7 ppm can be assigned to the aryl (Ar) carbon directly bonded to phosphorus (C_{Ar}–P),[19] and the peaks at 136.5, 132.4, 126.7 ppm can be unambiguously assigned to the sp^2 aromatic carbon atoms with hydrogen atoms (C_{Ar}–H) or the –CH group (C_{Ar}–CH).[20] Another two signals at approximately 40.8 and 44.8 ppm are the alkyl carbon atoms from –CH_2– and –CH–Ar, respectively.[21] Given that the SS ^{13}C NMR spectra for HC-TVP and HT-I are quite similar, the ^{31}P NMR spectra (Figure 1b) were further used to define the structure of the two polymers. For HT-I, the resonance at 29.5 ppm typically corresponded to the ionic phosphorous atoms, which is completely different from the signal at –5.6 ppm for the neutral phosphorous atoms of HC-TVP.[18,19,22] This result is consistent with the solution ^{31}P-NMR chemical shift of the model compound PPh_3-HI (Ph = phenyl; Figure S1 in the Supporting Information, SI), indicating the successful ionization of the phosphorous-based polymer frameworks after treatment with hydriodic acid. In the Fourier-transform IR (FT-IR) spectra of TVP, HC-TVP, and HT-I (Figure S2, SI), the peaks at 1633 and 830 cm^{-1} can be attributed to aromatic C = C and C–P stretching vibrations, respectively. For HT-I, the typical P–H vibration peak is at 880 cm^{-1}.[23] All of the above results indicated that HC-TVP and HT-I were successfully synthesized.

The porous nature of HC-TVP and HT-I were investigated by sorption analysis using nitrogen as the sorbate molecule. It was found that the isotherms of all the materials exhibited

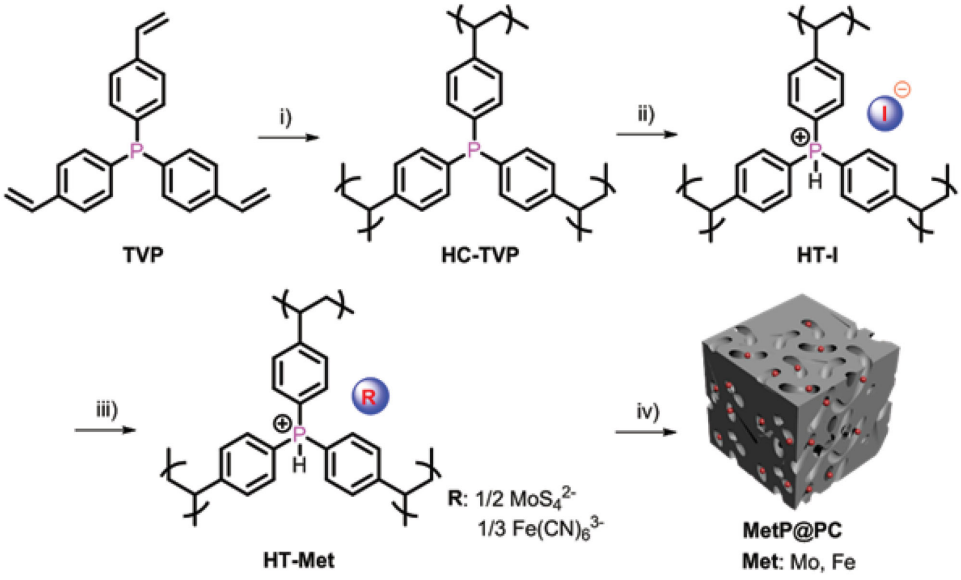

Scheme 1. Preparation of HT-Mets and related mesoporous carbons embedded with metal phosphides (MetP@PCs). Reaction conditions: i) AIBN, toluene, 65 °C, 24 h; ii) dioxane, aqueous hydriodic acid, room temperature (rt), 24 h; iii) $(NH_4)_2MoS_4$ or $K_3Fe(CN)_6$, DMF/water, 80 °C, 24 h; iv) H_2, 480 °C, 1 h, then annealed under argon at 1000 °C for 2 h.

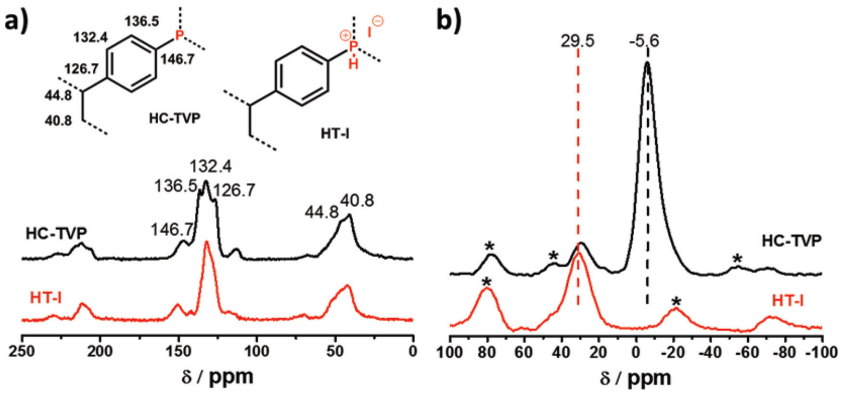

Figure 1. Solid-state ^{13}C NMR (a) and ^{31}P NMR (b) of HC-TVP and HT-I. Inset of (a) show the resonance assignment of the C centers on the chemical structures. Stars in (b) represent spinning sidebands.

type II nitrogen sorption according to IUPAC classifications (**Figure 2**a and Figure S3, SI; IUPAC = International Union of Pure and Applied Chemistry).[24] The specific surface areas for HC-TVP and HT-I are 901 and 596 $m^2\ g^{-1}$, respectively, on the basis of Brunauer–Emmett–Teller (BET) calculations. The distributions of the pore sizes are 5.36 and 9.66 nm for HC-TVP and HT-I, respectively, which were calculated by non-local density-functional-theory (NLDFT) methods. The differences of HC-TVP and HT-I in surface area and pore strucuture are likely to be a result of the fact that the continuous porous frameworks formed in HC-TVP might be sterically disrupted by the free iodide anions dispersed in the framework for HT-I. In comparison with HT-I, the specific surface area decreased after ion-exchange to 324 and 535 $m^2\ g^{-1}$ for HT-Mo and HT-Fe, respectively (**Table 1**). This result was reasonably ascribed to the partial pore filling and increase in mass.[19]

Porous polymers are considered good precursors for the confined formation of functional porous carbons, in which heteroatoms,[25] nanoparticles, and other species are introduced into the carbon framework; such a formation is required for various applications, e.g., energy storage and electrochemical catalysis.[26] Thermogravimetric analysis (TGA) confirmed that HC-TVP and HT-Met can be transformed into carbon materials with high carbon yields (30–60% at 800 °C; Figure S4, SI). Porous carbons that have MoP and FeP species embedded within (denoted as MoP@PC and FeP@PC, respectively) were prepared by the direct pyrolysis of HT-Mo and HT-Fe, respectively, at 480 °C for 1 h under a hydrogen atmosphere, and then at 1000 °C for 2 h under argon (Scheme 1). The specific surface areas of MoP@PC and FeP@PC further decreased relative to their polymer precursors, HT-Mo and HT-Fe, respectively, to 132 and 451 $m^2\ g^{-1}$, respectively (Table 1). The decrease in the surface areas for the MetP@PCs with respect to their corresponding HT-Met is probably due to the partial degradation of the polymer networks and recombination of fragments under the carbonization conditions.[25]

The successful formation of MoP@PC and FeP@PC were further verified by X-ray diffraction (XRD) analyses (**Figure 3**a,b). The series of peaks at $2\theta = 27.9°$, 32.2°, 43.1°, and 57.5° for MoP@PC can be assigned to the (001), (100), (101), and (110) facets of the MoP (International Centre for Diffraction Data (ICDD) Card No. 24–0771). FeP@PC shows the same XRD peaks as the orthorhombic cell of the FeP phase (ICDD Card No. 39–0809).

Transmission electron microscopy (TEM, **Figure 4**) was also used to reveal the microstructures of MetP@PC. The TEM images for MoP@PC and FeP@PC clearly show that the as-prepared materials are amorphous. Remarkably, large MetP particles are not evident in the higher-resolution TEM images, which indicate the uniform distribution of MetP in the porous carbon networks. According to the selective-area electron diffraction (SAED) analyses (Figure 4c,f), the (101), (001), (100), (110) facets[8e] for MoP@PC and the (020), (221), (201), (202) facets[9c,d] for FeP@PC can be easily calculated. These results are consistent with the XRD patterns in Figure 3a and b, respectively. Both MoP@PC and FeP@PC exhibit typical amorphous morphology without obvious crystallization (Figure 3c,d and Figure S5, SI). Uniform distributions of MoP and FeP in the composites were observed by SEM-EDX mapping (scanning electron microscopy (SEM) with energy-dispersive X-ray spectroscopy (EDX)) over a large region (Figure 3c,d). These results indicate that the phosphorous-containing polymer framework of HC-TVP serves as a reliable phosphorous precursor for the preparation of transition-metal phosphides. Undoubtedly, in this approach, the ionic phosphorous-containing porous polymers not only offer a uniformly distributed phosphorous source and abundant carbon source, but they also provide hydrophilic channels. These channels enable facile access for the metal-containing anions to the phosphonium cations in the network as a result of the electrostatic attraction in the ion-exchange process; this is likely beneficial to the uniform incorporation of the metal phosphide throughout the porous carbon, while under confined conditions.

X-ray photoelectron spectroscopy (XPS) analysis was carried out to determine the elemental composition of the as-prepared materials. The Mo 3d, P 2p, and S 2p spectra

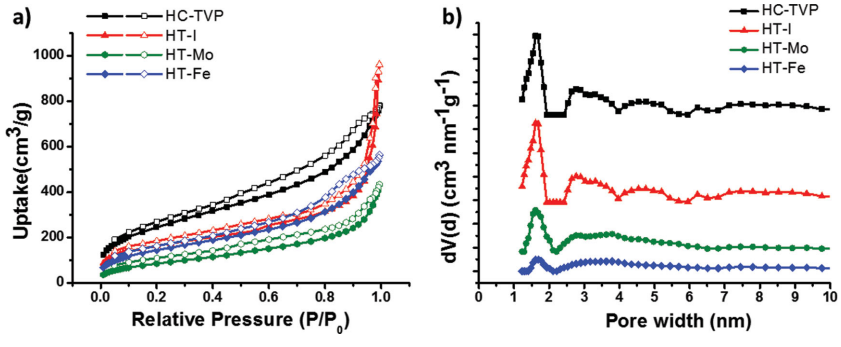

Figure 2. a) Nitrogen adsorption (filled symbols)/desorption (open symbols) isotherms at 77 K and b) pore size distribution for HC-TVP, HT-I, HT-Mo, and HT-Fe.

Table 1. Nitrogen physisorption properties of the prepared porous materials.

Sample	S_{BET} [a)] [$m^2 g^{-1}$]	S_{Lang} [b)] [$m^2 g^{-1}$]	S_{micro} [c)] [$m^2 g^{-1}$]	D_{av} [d)] [nm]	V_{micro} [e)] [$cm^3 g^{-1}$]	V_{tot} [f)] [$cm^3 g^{-1}$]	V_{micro}/V_{tot}
HC-TVP	901	1361	248	5.36	0.122	1.208	0.1
HT-I	596	825	143	9.66	0.052	1.439	0.04
HT-Mo	324	545	–	8.06	–	0.671	–
HT-Fe	535	812	113	6.37	0.053	0.853	0.06
MoP@PC	132	240	–	9.41	–	0.334	–
FeP@PC	451	625	198	3.76	0.094	0.325	–

[a)]Surface areas are calculated from the N_2 adsorption isotherm using the BET (S_{BET}, a) and Langmuir (S_{Lang}, [b)]methods; [c)]micropore surface area; [d)]average pore size based on the adsorption isotherm; [e)]micropore volume; [f)]total pore volume at $P/P_0 = 0.99$.

were obtained for HT-Mo and MoP@PC (**Figure 5**). The HT-Mo results exhibit two peaks at 232.6 and 228.8 eV in the Mo 3d spectrum, attributed to the Mo $3d_{3/2}$ and $3d_{5/2}$ binding energies for Mo^{4+}.[27] The two peaks at 162.7 and 161.2 eV, corresponding to the S $2p_{1/2}$ and $2p_{3/2}$ orbitals of divalent sulfide ions (S^{2-}), were observed, clearly demonstrating that I^- had been replaced by MoS_4^{2-}. The Mo 3d spectrum of MoP@PC showed two peaks at 230.4 and 227.1 eV ($3d_{3/2}$ and $3d_{5/2}$, respectively), essentially assigned to the molybdenum within a molybdenum phosphide.[2] The P 2p core level spectrum for MoP@PC indicates two peaks at 129.1 and 129.9 eV arising from the P in MoP.[2,4] The Fe 2p, P 2p, and N 1s spectra for HT- Fe and FeP@PC are illustrated in Figure 5d–f. For HT-Fe, two peaks at 725.0 and 721.0 eV in the Fe 2p spectrum were assigned to Fe^{3+} and Fe^{2+}. The existence of Fe^{2+} indicates that the Prussian-Blue (PB; Figure S6, SI) by-product was formed in anion-exchange processing. In the N 1s spectrum of HT-Fe, two peaks at around 399.2 and 397.9 eV, can be assigned to the

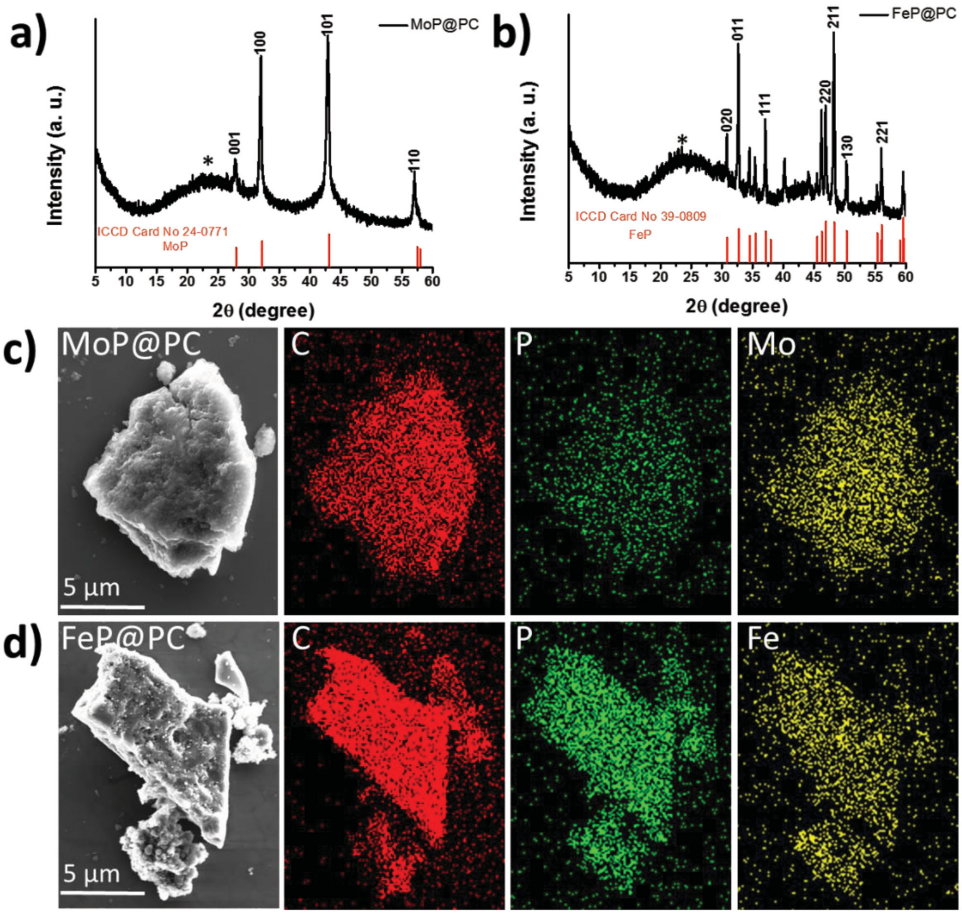

Figure 3. a,b) XRD patterns for MoP@PC (a) and FeP@PC (b); * indicate the presence of amorphous porous carbon; c,d) SEM images and SEM elemental mappings of MoP@PC (c) and FeP@PC (d).

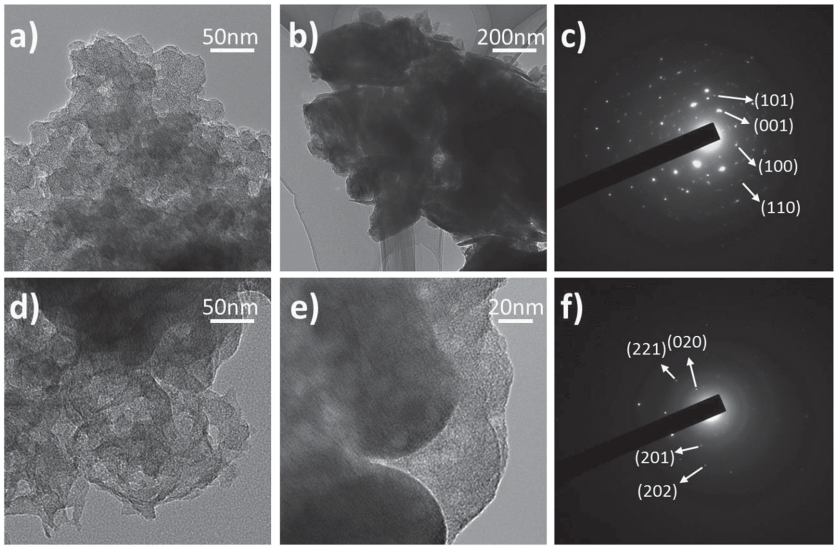

Figure 4. a,b) TEM images and c) SAED pattern of MoP@PC; d,e) TEM image and f) SAED pattern of FeP@PC.

N of $Fe(CN)_6^{4-}$ and $Fe(CN)_6^{3-}$, respectively.[28] For FeP@PC, the Fe 2p spectrum shows two pairs of peaks (Fe $2p_{3/2}/2p_{1/2}$) at the binding energies of 707.2/720.3 and 710.8/725.6 eV, which can be assigned to the Fe–P and Fe–O bonds, respectively. The residual oxidized Fe species is probably from the superficial oxidation of FeP@PC in air.[9a] The P 2p spectrum shows two small peaks at 128.9 and 129.6 eV, and one strong peak at 132.8 eV, which can be assigned to the P–C and P–Fe bonds, respectively.[29] These results indicated that this new approach is a successful way to uniformly incorporate metal phosphides in porous carbons. The XPS survey spectra for HC-TVP, HT-I, HT-Mo, HT-Fe, MoP@PC, and FeP@PC are available in the SI (Figure S7). The phosphorus content (atomic%, Table S1, SI) based on the XPS analyses was calculated for HC-TVP (4.47%), HT-I (4.72%), HT-Mo (2.66%), HT-Fe (1.71%), MoP@PC (3.61%), and FeP@PC (8.07%). Inductively coupled plasma (ICP) analysis further confirmed the loading amount of Mo and Fe on the polymer networks at 4.5% and 4.8%, for MoP@PC and FeP@PC, respectively.

Recent studies indicate that transition-metal phosphides are one of the best kinds of catalysts for the HER.[2,3c,9a] The electrochemically catalyzed HERs for MetP@PC and the commercial Pt/C catalyst were carried out in 0.50-M H_2SO_4 solution at a scan rate of 5 mV s^{-1} using a typical three-electrode set-up at room temperature (**Figure 6**). The polarization curves without *iR* compensation (*iR* = current*resistance) are shown in Figure 6a,b. MoP@PC exhibited a very small onset overpotential of ≈48 mV and current densities of 2, 10, and 100 mA cm^{-2} at overpotentials of 13, 47, and 226 mV, respectively. FeP@PC also showed promising catalytic activities for the HER under the same experimental conditions; the current densities reached 2, 10, and 100 mA cm^{-2} at the overpotentials of 21, 52, and 267 mV, respectively. These results are superior to those of the previously reported MoP nanoparticles,[8d] MoP/S,[2] MoP,[4,14] and FeP nanosheets[15] (Table S2, SI).

Stability is another critical issue for electrocatalysts; thus, the durability of the catalytic response was measured by testing MoP@PC continuously for 4000 cycles (Figure 6c) in

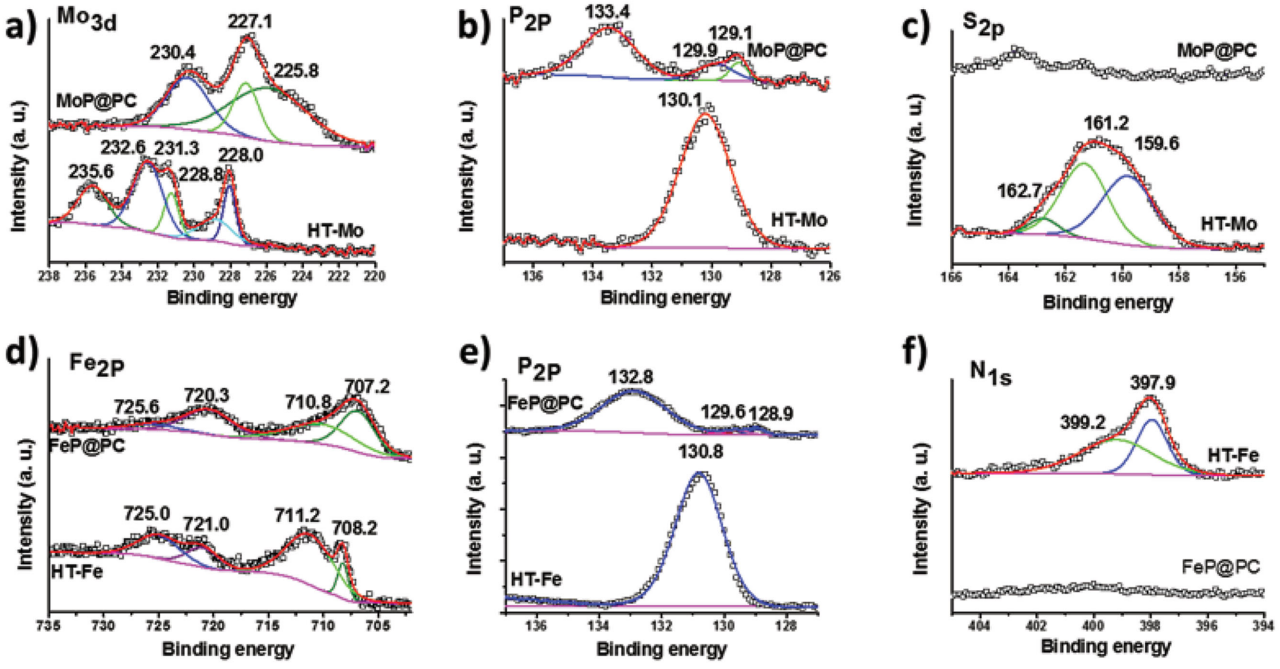

Figure 5. The Mo 3d (a), P 2p (b) and S 2p (c) core level spectra of HT-Mo and MoP@PC; The Fe 2p (d), P 2p (e) and S 2p (f) core level spectra of HT-Fe and FeP@PC. Binding energy unit: eV; hollow squares: experimental data; solid lines: fitted data.

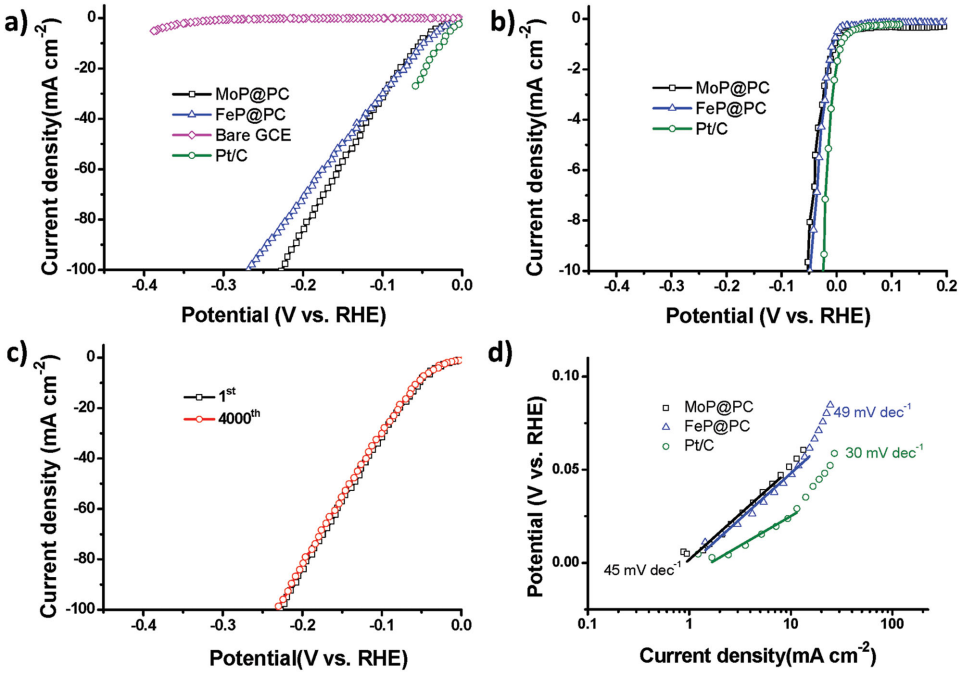

Figure 6. a,b) Polarization curves of bare glassy carbon electrode (GCE), MoP@PC, FeP@PC, and Pt/C. c) Polarization curves of MoP@PC before and after 4000 cycles in 0.5-M H_2SO_4. d) Tafel plots of MoP@PC, FeP@PC, and Pt/C.

the range of +0.20 to –0.50 V versus the reversible hydrogen electrode (vs. RHE) at a scan rate of 100 mV s^{-1}. MoP@PC exhibited a slight loss in the cathodic current density, which possesses superior stability in a long-term electrochemical process over the reported results of MoP-based materials, such as MoP nanoparticles,[8d] MoP/S,[2] and amorphous MoP nanoparticles.[8e] FeP@PC had similar results as MoP@PC (Figure S8, SI). The Tafel plots for MoP@PC and Pt/C are in Figure 6d. According to the Tafel equation ($\eta = b \log j + a$, where η is the iR-corrected potential, a is the Tafel constant, b is the Tafel slope, and j is the current density), the Tafel slopes for MoP@PC and Pt/C were calculated to be ≈45 and ≈30 mV dec^{-1}, respectively, which is superior to that of FeP@PC (49 mV dec^{-1}). The Tafel slopes for MoP@PC and FeP@PC did not reach the Tafel slopes of 29 (between 25 and 125 mV) and 38 (between 150 and 200 mV) mV dec^{-1}, respectively, which are correlated with the different rate-determining steps of the HER.[13c] This result revealed that for MoP@PC and FeP@PC, the HER proceeds via a Volmer–Heyrovsky mechanism.[30]

The outstanding HER activities for MoP@PC and FeP@PC can be attributed to the following reasons: 1) their high specific surface areas offer many catalytic active sites,[31] and 2) integration of the uniformly distributed[32] MoP or FeP and the hierarchical porous structure[8d] in the carbon framework is likely favorable for the fast mass transport of reactants and products, and it also improves the electrical conductivity for facile electron transfer.[17]

3. Conclusion

In summary, a novel phosphorus-containing hyper-crosslinked porous polymer (HC-TVP) was efficiently prepared from tris(4-vinylphenyl)phosphane by radical polymerization. HC-TVP was readily transformed into the cationic porous polymer (HT-I) by treatment with HI. Transition-metal-containing anions, such as tetrathiomolybdate (MoS_4^{2-}), and hexacyanoferrate ($Fe(CN)_6^{3-}$), can be easily incorporated into the cationic porous polymer (HT-I) by an ion-exchange process to form porous polymers loaded with metal-containing anions. After pyrolysis under hydrogen atmosphere, these loaded polymers were then efficiently converted at a large scale to porous carbons with a uniform distribution of embedded metal phosphides (MetP@PCs, Met = Mo, Fe). The achieved MetP@PCs exhibited excellent electrocatalytic activity for the hydrogen evolution reaction (HER) under acidic conditions; the activity was comparable to that of the commercially available Pt/C catalyst. This approach offers a new pathway to the confined preparation of MetP@PCs based on a variety of transition metals, which may be applicable in catalysis and energy conversion and storage.

4. Experimental Section

All chemicals were purchased from Aladdin, Adamas, and Aldrich. All air-sensitive reactions were carried out under nitrogen atmosphere and using Schlenk techniques. All solvents were dried before use.

Preparation of TVP: TVP was prepared using slight modifications to the preparation found in the literature.[18] Mg turnings (1.31 g, 54 mmol, 5.4 eq (equivalents)) and tetrahydrofuran (THF; 24 mL) were mixed in a 100-mL round-bottom flask under inert atmosphere. 1,2-Dibromoethane (10 µL) was added to the mixture. *p*-Chlorostyrene (4.99 g, 36 mmol, 3.6 eq) was then added dropwise, and the resulting mixture was stirred at 60 °C for 3 h. Then, PCl_3 (1.37 g, 10 mmol, 1 eq) was added dropwise, and the solution was stirred at room temperature for 6 h. To terminate the reaction, aqueous NH_4Cl was added. The organic layer was separated, and the aqueous layer was extracted with Et_2O (diethyl

ether). The combined organic phases were washed with water and dried over $MgSO_4$, filtered, and concentrated. The crude product was purified by silica gel chromatography (4:1 hexanes:CH_2Cl_2) to give TVP as a white solid (2.04 g, 60% yield). ^{1}H NMR (500 MHz, $CDCl_3$, δ): 7.45–7.25 (m, 4H), 6.73 (dd, J = 17.6, 10.9 Hz, 1H), 5.81 (d, J = 17.6 Hz, 1H), 5.31 (d, J = 10.9 Hz, 1H). ^{31}P NMR (162 MHz, $CDCl_3$, δ): –5.64 (s).

Synthesis of HC-TVP: TVP (500 mg, 1.47 mmol) and AIBN (10 mg, 0.06 mmol) were mixed together in a dry 100-mL round-bottom flask under inert atmosphere. Toluene (30 mL) was added to the mixture via syringe. The reaction was stirred at 65 °C for 24 h. Then the obtained white solid was filtered and dried under vacuum at 60 °C for 24 h (yield: >90%).

Synthesis of HT-I:[33] HC-TVP (1.05 g) was mixed with dioxane (8 mL) in a 25-mL round-bottom flask. Aqueous 55% hydroiodic acid (1 mL) was added to the mixture. The white dispersion was stirred at room temperature for 24 h. An orange solid was obtained after filtration. After diethyl ether washing and drying under vacuum at 60 °C for 24 h, the ionic polymer framework (HT-I) was obtained.

Typical Synthesis of HT-Met (Met = Mo, Fe):[19] HT-I (200 mg) was mixed with $(NH_4)_2MoS_4$ or $K_3Fe(CN)_6$ in water (5 mL) at 80 °C for 12 h; this was followed by immersion in deionized water for 24 h. Then, a deeply colored solid (HT-Met, Met = Mo, Fe) was obtained by filtration and drying under vacuum at 60 °C for 24 h.

Pyrolysis of HT-Met: The dried HT-Met was grounded into a fine powder before pyrolysis at a heating rate of 10 °C min^{-1} up to 480 °C and then held for 1 h under a hydrogen atmosphere. Then the temperature was risen to 1000 °C and maintained for another 2 h under argon. After the temperature return to room temperature, the final product was recovered; in the text, it has been denoted as MetP@PC (Met = Mo, Fe).

Synthesis of Model Compound Triphenylphosphine hydroiodide (PPh_3-HI):[33] Triphenylphosphine (1.05 g) was dissolved in dioxane (8 mL) in a 25-mL round-bottom flask. Then, 55% aqueous hydroiodic acid (1 mL) was added. The mixture was stirred at room temperature for 24 h. The orange solid was obtained after filtration and washing with diethyl ether. After drying under vacuum for 12 h at 40 °C, the final product was isolated without any further purification (yield: ≈99%). ^{1}H NMR (400 MHz, DMSO-d_6, δ): 7.60 (ddd, J = 11.5, 8.1, 4.1 Hz, 1H), 7.56–7.50 (m, 1H), 4.31 (s, 1H). ^{31}P NMR (162 MHz, DMSO-d_6, δ): 26.65 (s). HRMS (ESI) m/z 263.1 $[M - I]^+$.[34]

Characterization: Solid-state ^{13}C NMR analysis was conducted on a Bruker AVANCE III 300 Spectrometer. Samples were spun at 5 kHz in a 4-mm zirconium rotor within a magic-angle spinning (MAS) probe. An acquisition time of 20 ms, a contact time of 1 ms, and a 6.5-μs pre-scan delay were used. The recycle time was 2 s in order to obtain fully relaxed spectra. Chemical shifts were externally referenced to adamantane at 38.48 ppm. FT-IR spectroscopy was performed on a Spectrum 100 (Perkin Elmer, Inc., USA) spectrometer with a scan range of 4000–400 cm^{-1}. The sample powders were pulverized with KBr and pressed into disks. TGA of the samples was performed using a Q5000IR (TA Instruments, USA) thermogravimetric analyzer at a heating rate of 20 °C min^{-1} under nitrogen flow. SEM was performed using FEI Sirion-200 (FEI Co., USA) field-emission scanning electron microscope. XRD measurements were performed using a Rigaku D/Max 2500 X-ray diffractometer with Cu Kα radiation (k = 1.54 Å) at a generator voltage of 40 kV and a generator current of 50 mA with a scanning speed of 5° min^{-1} from 5° to 80°. XPS was performed using an AXIS Ultra DLD system (Kratos Co., Japan) with Al Kα radiation as the X-ray source. The gas sorption isotherms were measured via an Auto-sorb-iQA3200–4 sorption analyzer (Quantatech Co., USA) based on N_2 adsorption.

Electrochemical Measurements: Electrochemical measurements (CV (cyclic voltammetry) and RDE (using a rotating disk electrode)) were conducted using an AFMSRCE 2759 advanced electrochemical system (Pine Instrument Co., USA). A three-electrode cell system was employed incorporating a rotating glass carbon disk and a platinum ring electrode (Pine Instrument Co., USA) afer loading the electrocatalyst as the working electrode, an Ag/AgCl (KCl, 3 M) electrode as the reference electrode, and a carbon rod as the counter-electrode. All potentials were recorded with respect to the RHE. Catalyst ink was typically made by dispersing 5 mg of catalyst in 0.5 mL of 0.05 wt.% Nafion solution (Gashub, Singapore) and ultrasonicating the subsequent mixture; an aliquot of 6 μL was pipetted onto the glassy carbon electrode (0.2471 cm^{-2}) to reach a catalyst loading of 0.243 mg cm^{-2}. In all measurements, the Ag/AgCl reference electrode was calibrated with respect to the RHE. Linear-sweep voltammetry (LSV) measurements were conducted in 0.5-M H_2SO_4 at a scan rate of 5 mV s^{-1}. All potentials reported were calibrated to the RHE. In 0.5-M H_2SO_4, E (RHE) = E (Ag/AgCl) + 0.214 V, where E is the potential of the electrode.

Supporting Information

Supporting Information (NMR, FT-IR, XRD, XPS, and HER performance) is available from the Wiley Online Library or from the author.

Acknowledgements

S.H. and Y.F. contributed equally to this research. The work was financially supported by the National Basic Research Program of China (973 Program: 2013CBA01602, 2012CB933404), the Natural Science Foundation of China (51403126 and 21174083), and Shanghai Jiao Tong University (211 and 985 Project). We thank the Instrumental Analysis Center of Shanghai Jiao Tong University for providing some measurements.

Received: April 7, 2015
Published online: May 15, 2015

[1] J. A. Turner, *Science* **2004**, *305*, 972.
[2] J. Kibsgaard, T. F. Jaramillo, *Angew. Chem. Int. Ed.* **2014**, *53*, 14433.
[3] a) V. Artero, J. M. Saveant, *Energy Environ. Sci.* **2014**, *7*, 3808; b) L. Chen, M. Wang, K. Han, P. L. Zhang, F. Gloaguen, L. C. Sun, *Energy Environ. Sci.* **2014**, *7*, 329; c) C. G. Morales-Guio, L.-A. Stern, X. Hu, *Chem. Soc. Rev.* **2014**, *43*, 6555.
[4] P. Xiao, M. A. Sk, L. Thia, X. M. Ge, R. J. Lim, J. Y. Wang, K. H. Lim, X. Wang, *Energy Environ. Sci.* **2014**, *7*, 2624.
[5] a) R. K. Das, Y. Wang, S. V. Vasilyeva, E. Donoghue, I. Pucher, G. Kamenov, H.-P. Cheng, A. G. Rinzler, *ACS Nano* **2014**, *8*, 8447; b) W. Cui, Q. Liu, N. Cheng, A. M. Asiri, X. Sun, *Chem. Commun.* **2014**, *50*, 9340.
[6] Y. Zheng, Y. Jiao, L. H. Li, T. Xing, Y. Chen, M. Jaroniec, S. Z. Qiao, *ACS Nano* **2014**, *8*, 5290.
[7] a) Y. Zhao, F. Zhao, X. Wang, C. Xu, Z. Zhang, G. Shi, L. Qu, *Angew. Chem. Int. Ed.* **2014**, *53*, 13934; b) M. Shalom, S. Gimenez, F. Schipper, I. Herraiz-Cardona, J. Bisquert, M. Antonietti, *Angew. Chem. Int. Ed.* **2014**, *53*, 3654.
[8] a) W. Cui, N. Y. Cheng, Q. Liu, C. J. Ge, A. M. Asiri, X. P. Sun, *ACS Catal.* **2014**, *4*, 2658; b) L. F. Pan, Y. H. Li, S. Yang, P. F. Liu, M. Q. Yu, H. G. Yang, *Chem. Commun.* **2014**, *50*, 13135; c) Z. Chen, D. Cummins, B. N. Reinecke, E. Clark, M. K. Sunkara, T. F. Jaramillo, *Nano Lett.* **2011**, *11*, 4168; d) Z. C. Xing, Q. Liu, A. M. Asiri, X. P. Sun, *Adv. Mater.* **2014**, *26*, 5702; e) J. M. McEnaney, J. C. Crompton, J. F. Callejas, E. J. Popczun, A. J. Biacchi, N. S. Lewis, R. E. Schaak, *Chem. Mater.* **2014**, *26*, 4826; f) W. Cui, Q. Liu, Z. Xing, A. M. Asiri, K. A. Alamry, X. Sun, *Appl. Catal. B: Environ.* **2015**, *164*, 144.
[9] a) P. Jiang, Q. Liu, Y. Liang, J. Tian, A. M. Asiri, X. Sun, *Angew. Chem. Int. Ed.* **2014**, *53*, 12855; b) Z. Zhang, B. Lu, J. Hao, W. Yang, J. Tang, *Chem. Commun.* **2014**, *50*, 11554; c) J. F. Callejas, J. M. McEnaney, C. G. Read, J. C. Crompton, A. J. Biacchi,

E. J. Popczun, T. R. Gordon, N. S. Lewis, R. E. Schaak, *ACS Nano* **2014**, *8*, 11101; d) J. Tian, Q. Liu, Y. Liang, Z. Xing, A. M. Asiri, X. Sun, *ACS Appl. Mater. Interfaces* **2014**, *6*, 20579; e) Q. Liu, Z. Pu, A. M. Asiri, X. Sun, *Electrochim. Acta* **2014**, *149*, 324.

[10] a) Q. Liu, J. Q. Tian, W. Cui, P. Jiang, N. Y. Cheng, A. M. Asiri, X. P. Sun, *Angew. Chem. Int. Ed.* **2014**, *53*, 6710; b) L. G. Bloor, P. I. Molina, M. D. Symes, L. Cronin, *J. Am. Chem. Soc.* **2014**, *136*, 3304; c) Z. H. Pu, Q. Liu, P. Jiang, A. M. Asiri, A. Y. Obaid, S. P. Sun, *Chem. Mater.* **2014**, *26*, 4326; d) J. Tian, Q. Liu, A. M. Asiri, X. Sun, *J. Am. Chem. Soc.* **2014**, *136*, 7587; e) J. Tian, N. Cheng, Q. Liu, W. Xing, X. Sun, *Angew. Chem. Int. Ed.* **2015**, *54*, 5493.

[11] a) C. G. Morales-Guio, L. Liardet, M. T. Mayer, S. D. Tilley, M. Gratzel, X. Hu, *Angew. Chem. Int. Ed.* **2014**, *54*, 664; b) J. Q. Tian, Q. Liu, N. Y. Cheng, A. M. Asiri, X. P. Sun, *Angew. Chem. Int. Ed.* **2014**, *53*, 9577.

[12] a) J. M. McEnaney, J. C. Crompton, J. F. Callejas, E. J. Popczun, C. G. Read, N. S. Lewis, R. E. Schaak, *Chem. Commun.* **2014**, *50*, 11026; b) S. T. Hunt, T. Nimmanwudipong, Y. Roman-Leshkov, *Angew. Chem. Int. Ed.* **2014**, *53*, 5131; c) Z. Pu, Q. Liu, A. M. Asiri, X. Sun, *ACS Appl. Mater. Interfaces* **2014**, *6*, 21874; d) Z. Xing, Q. Liu, A. M. Asiri, X. Sun, *ACS Catal.* **2015**, *5*, 145.

[13] a) Z. H. Pu, Q. Liu, C. Tang, A. M. Asiri, X. P. Sun, *Nanoscale* **2014**, *6*, 11031; b) Y. F. Xu, M. R. Gao, Y. R. Zheng, J. Jiang, S. H. Yu, *Angew. Chem. Int. Ed.* **2013**, *52*, 8546; c) E. J. Popczun, J. R. McKone, C. G. Read, A. J. Biacchi, A. M. Wiltrout, N. S. Lewis, R. E. Schaak, *J. Am. Chem. Soc.* **2013**, *135*, 9267; d) P. Jiang, Q. Liu, X. Sun, *Nanoscale* **2014**, *6*, 13440.

[14] X. B. Chen, D. Z. Wang, Z. P. Wang, P. Zhou, Z. Z. Wu, F. Jiang, *Chem. Commun.* **2014**, *50*, 11683.

[15] Y. Xu, R. Wu, J. Zhang, Y. Shi, B. Zhang, *Chem. Commun.* **2013**, *49*, 6656.

[16] P. Jiang, Q. Liu, C. J. Ge, W. Cui, Z. H. Pu, A. M. Asiri, X. P. Sun, *J. Mater. Chem. A* **2014**, *2*, 14634.

[17] H. F. Du, Q. Liu, N. Y. Cheng, A. M. Asiri, X. P. Sun, C. M. Li, *J. Mater. Chem. A* **2014**, *2*, 14812.

[18] T. Iwai, T. Harada, K. Hara, M. Sawamura, *Angew. Chem. Int. Ed.* **2013**, *52*, 12322.

[19] Q. Zhang, S. Zhang, S. Li, *Macromolecules* **2012**, *45*, 2981.

[20] D. Wang, W. Yang, L. Li, X. Zhao, S. Feng, H. Liu, *J. Mater. Chem. A* **2013**, *1*, 13549.

[21] G. J. Summers, R. B. Maseko, C. A. Summers, *Polym. Int.* **2014**, *63*, 1785.

[22] Q. Zhang, Y. Yang, S. Zhang, *Chem. Eur. J.* **2013**, *19*, 10024.

[23] M. A. Khan, D. G. Tuck, M. J. Taylor, D. Rogers, *J. Crystallogr. Spectrosc. Res.* **1986**, *16*, 895.

[24] K. S. W. Sing, D. H. Everett, R. A. W. Haul, L. Moscou, R. A. Pierotti, J. Rouquerol, T. Siemieniewska, *Pure Appl. Chem.* **1985**, *57*, 603.

[25] a) X. Zhuang, F. Zhang, D. Wu, N. Forler, H. Liang, M. Wagner, D. Gehrig, M. R. Hansen, F. Laquai, X. Feng, *Angew. Chem. Int. Ed.* **2013**, *52*, 9668; b) X. Zhuang, F. Zhang, D. Wu, X. Feng, *Adv. Mater.* **2014**, *26*, 3081; c) X. Zhuang, Y. Mai, D. Wu, F. Zhang, X. Feng, *Adv. Mater.* **2015**, *27*, 403; d) Y. Zhang, X. Zhuang, Y. Su, F. Zhang, X. Feng, *J. Mater. Chem. A* **2014**, *2*, 7742.

[26] C. Cao, X. Zhuang, Y. Su, Y. Zhang, F. Zhang, D. Wu, X. Feng, *Polym. Chem.* **2014**, *5*, 2057.

[27] Y. H. Chang, C. T. Lin, T. Y. Chen, C. L. Hsu, Y. H. Lee, W. J. Zhang, K. H. Wei, L. J. Li, *Adv. Mater.* **2013**, *25*, 756.

[28] a) J. Qu, S. Kang, X. Du, T. Lou, J. Qu, *Electroanalysis* **2013**, *25*, 1722; b) J. Sanetuntikul, S. Shanmugam, *Electrochim. Acta* **2014**, *119*, 92.

[29] A. A. Muleja, X. Y. Mbianda, R. W. Krause, K. Pillay, *Carbon* **2012**, *50*, 2741.

[30] a) B. E. Conway, B. V. Tilak, *Electrochim. Acta* **2002**, *47*, 3571; b) N. Pentland, J. O. M. Bockris, E. Sheldon, *J. Electrochem. Soc.* **1957**, *104*, 182.

[31] J. Kibsgaard, Z. Chen, B. N. Reinecke, T. F. Jaramillo, *Nat. Mater.* **2012**, *11*, 963.

[32] S. T. Oyama, T. Gott, H. Zhao, Y.-K. Lee, *Catal. Today* **2009**, *143*, 94.

[33] N. Aoyagi, Y. Furusho, T. Endo, *Tetrahedron Lett.* **2013**, *54*, 7031.

[34] a) R. Zhang, D. N. Harischandra, M. Newcomb, *Chemistry* **2005**, *11*, 5713; b) M. H. Haukaas, G. A. O'Doherty, *Org. Lett.* **2001**, *3*, 4014.